C80-119

Effect of Nozzle Spacing on Ground Interference Forces for a Two-Jet V/STOL Aircraft

00001
00006
20007

William G. Hill Jr.* and Richard C. Jenkins†
Grumman Aerospace Corporation, Bethpage, N.Y.

The effect of nozzle spacing on ground interference forces in hover was investigated for a two-jet V/STOL aircraft design. Interference forces showed a complicated behavior with nozzle spacing, fuselage geometry, and height above ground. For some conditions a slight change in nozzle spacing resulted in a fourfold change in the interference force, from 3 to 12% of the basic jet thrust. An understanding of the observed aircraft force behavior was developed using detailed measurements of the upwash flow properties, along with force and pressure measurements on a series of two-dimensional fuselage representations.

Nomenclature

D = nozzle exit diameter
ΔF = interference force on vehicle (total force minus thrust)
H = nozzle height above ground
$\dot{M}_\theta$ = flow momentum flux per radian
P = pressure
q = dynamic pressure $(P_t - P_s)$
r = radius of fuselage lower corners
S = nozzle separation distance
T = jet thrust
W = width of fuselage cross section
x,y,z = coordinates, see Fig. 6
σ = strake depth from fuselage bottom

Subscripts

a = ambient
j = jet exit
t = total
s = static

Introduction

THE interference forces that occur when a V/STOL aircraft operates in hover or during landing and takeoff form one of the most critical conditions for aircraft design.[1] The fluid mechanics involved in the creation of these forces is quite complex, involving three-dimensional, turbulent flows and both free shear flows and fluid/surface interactions. Platzer and Margason[2] presented a review of the 1975 V/STOL aerodynamics workshop[3] which summarized the state-of-the-art at that time. Proceedings of similar workshops held in 1977 and 1979 are also available.[4-6] The spacing between nozzles plays several interacting roles for the designer. Wide nozzle spacing produces more control moment power, but also generally requires more structural weight and complexity. It can also affect the interference forces greatly, adding to the tradeoff problems. The flow complexity and the large number of parameters affecting the forces and moments demand a wide range of variables and a large amount of experimentation in order to obtain sufficient data for modeling these flows.

Presented as Paper 79-1856 at the AIAA Aircraft Systems and Technology Conference, New York, N.Y., Aug. 20-22, 1979; submitted Oct. 1, 1979; revision received Feb. 1, 1980.

Index categories: Aerodynamics; Configuration Design; Jets, Wakes, and Viscid-Inviscid Flow Interactions.

*Staff Scientist, Research Dept.
†Research Scientist, Research Dept. Member AIAA.

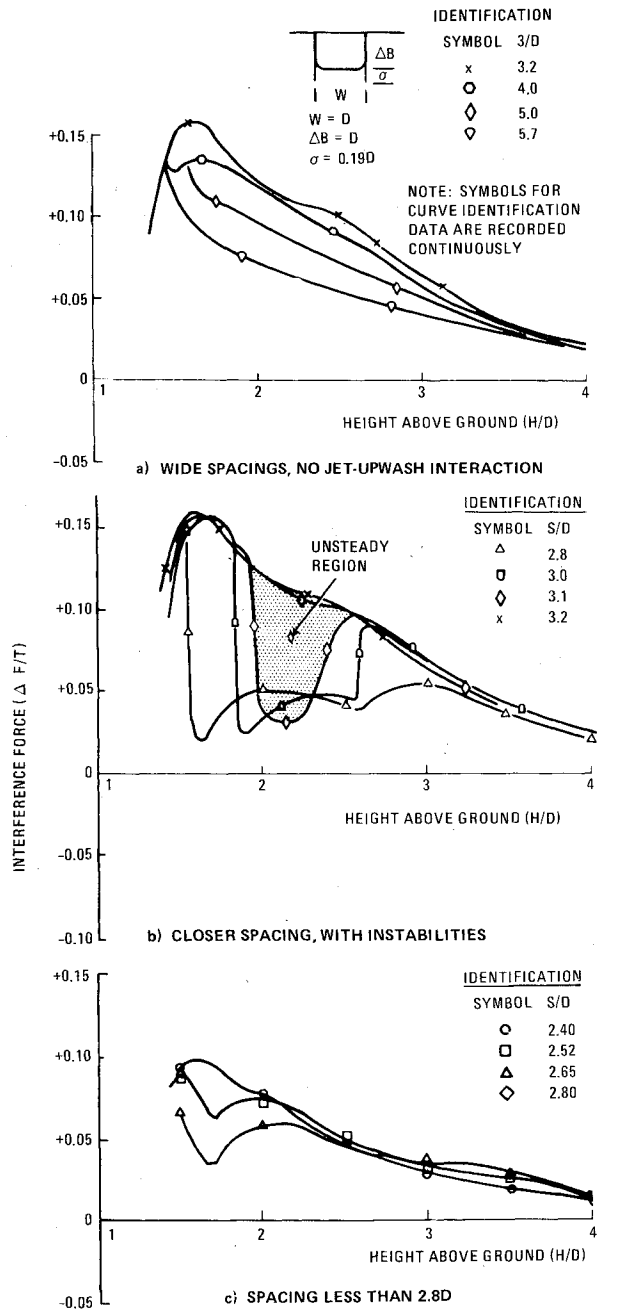

Fig. 1 Effect of jet spacing on IGE forces for two jet aircraft with strakes.

Our approach to this problem has been to utilize low-speed, cold jets and small-scale models. While differences probably exist in the magnitude of the flow properties between tests of scale models and those of full-scale engines and vehicles, we believe that these tests capture the fundamental nature of the flow. In our search for data to evaluate this premise, we have found only a few applicable cases. Our own work on the wall jet from an impinging fan jet engine, using a 1/14 scale cold jet model, showed excellent agreement with data from a Hamilton-Standard Q-fan engine.[7] A report by Wooten and Hoff[8] showed no effect of pressure ratio on a supersonic V/STOL design, while the data of Gentry and Margason[9] and Spreeman and Sherman[10] show a moderate effect, as correlated by Kuhn.[11] The absence of documented full-scale data with detailed flowfield properties makes the assessment of scale effects difficult.

References 12-14 describe the development of techniques used by Grumman to predict pressure distributions and aerodynamic characteristics for V/STOL aircraft operating both in and out of ground effect. The wide range of Grumman efforts has been coordinated around a computer program using a modular, or building block, approach to compute the induced forces and moments.[6] We have also found that models developed for the effects of individual parameters can be very helpful to the designer directly by indicating the general trends to be expected.

Experimental Apparatus

The ground interaction flows were produced by impingement of two axisymmetric, subsonic air jets from a low-turbulence level setting chamber. The nozzles were 5.08 cm i.d. tubes with a constant-diameter length of 28 cm and had an elliptic entrance contour (as in ASME flow-metering nozzles). Velocity profiles taken at the nozzle exit plane showed 91.4 m/s uniform velocity surrounded by a 0.63 cm thick turbulent boundary layer. The thrust of both nozzles deduced from these profiles ($T=36.4$ N) was used to normalize interference force curves.

A sting balance was used to measure ground interference forces on the aircraft model and on two-dimensional models. Forces on the large exit plane plate were measured with three separate strain gage force beams. Ground pressure profiles were obtained by displacing the ground plane parallel to its surface. Flow properties in the upwash were measured with a Kiel probe and a static probe spaced closely enough so that the dynamic pressure could be determined from the difference in measured pressure. Force and pressure measurements were displayed on an X-Y recorder to provide a continuous data plot vs either ground height or probe location.

Interference Forces

Aircraft Model

The aircraft design used in this study was described in Ref. 15. This aircraft is one version of Grumman design 698, aimed at the Navy Type A V/STOL (subsonic ASW, AEW) mission. Reference 15 indicated that our scale of experiment produces results consistent with those of larger scale facilities.

A series of experiments with the basic airplane showed interference force levels becoming more negative as the jets were brought closer together, down to a nozzle spacing to diameter (S/D) ratio of 2.8. Below 2.8, down to 2.4 (the limit of our apparatus), the force curves stayed essentially constant.

When strakes were added (illustrated as a depth σ on Fig. 1) a much more complicated situation developed. For aid in observing and understanding the behavior, these data are presented in a series of three graphs in Fig. 1. Gear height is the value of H/D when the aircraft is on the ground. Figure 1a shows that beginning at moderately wide spacings ($S/D=5.7$) the interference forces ($\Delta F/T$) are positive over the range of H/D investigated. As the jet spacing is decreased, the forces become larger up to a spacing of $S/D\approx 4$, and then stay approximately constant to $S/D=3.2$. Going to Fig. 1b (carrying over the curve for $H/D=3.2$) we found that at a spacing of $S/D=3.1$ the flow became very unsteady for heights between approximately $H/D=1.8$ and 2.4. The force levels varied over the range indicated in the shaded area of the figure. As the spacing decreased still further, this unsteady behavior disappeared, but a region near these same H/D's occurred where the force fell from the $S/D=3.2$ value to a much lower value. The width (in H/D values) of this region of lowered forces grew wider as S/D was decreased until for spacings less than $S/D=2.8$ the higher force region did not occur at all. From this point on the general force level again showed a slight increase with closer spacings down to $S/D=2.4$.

The changes in general level and shape of these interference forces with strakes were found to be a property of the upwash flow itself, rather than its interaction with the aircraft. The upwash flow, even without a vehicle present, was found to be unstable for spacings of $S/D\approx 3$ and height above ground H/D between 1.5 and 2.5. Results of upwash flow measurements are given later in this paper.

All of the above experiments were conducted with one specific aircraft design. We had earlier found that details of the body geometry could strongly affect the interference forces also. An example of this is the effect of the fuselage corner radius, as shown in Ref. 16. Changing the corner to a sharper one brought positive interference forces.

To perform a systematic investigation of these effects of body geometry, we used several series of simplified bodies, as well as extensive measurements and modeling of the basic jet/upwash flows.

Two-Dimensional Body Forces

Our first series of experiments involved a series of cylindrical bodies similar to the aircraft fuselage in the previous section. These bodies had one nozzle diameter width, a semicylindrical upper surface, and a bottom surface of variable cross-sectional shape.

The first area addressed was the effect of the lower surface contour. The basic discovery in this area was a change between attached flow around the body and separation at the lower corner as the corner radius was changed. Flow visualization using tufts show this behavior clearly. The switch between attached and separated flow was found at a corner radius to body width (r/w) of 0.188. At this radius either flow could exist, and could be switched by disturbance of the flow.

The effect of corner radius on the interference forces is shown in Fig. 2. Beginning from a sharp corner which results in a large positive interference force, the force decreases as the

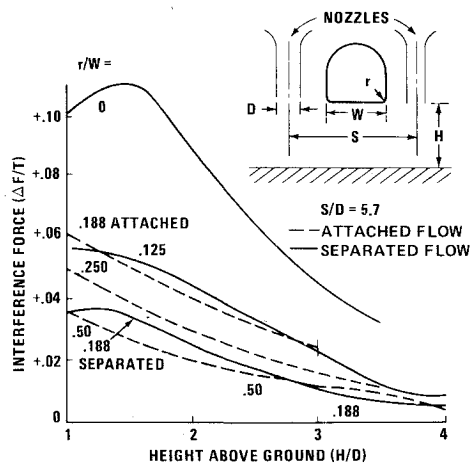

Fig. 2 Effect of corner radius on IGE forces—two-dimensional bodies.

corner radius is increased. When the flow switches from separation at the corners to attached flow ($r/w = 0.188$), the force jumps upward to a larger value. Further increase in the radius results in a return to the trend of decreasing force with increasing radius.

The occurrence of a larger upward force (body "drag" in the upwash flow) for attached flow than for separated flow is contrary to normal aerodynamic drag experience for a body in an infinite stream. The pressure distributions of Fig. 3 help to explain this behavior. The pressures on both the lower surface and the upper surface are affected by the change from separated to attached flow. The pressure on the upper surface is very near ambient when the flow is separated; for a body in an infinite stream, this surface would experience the "base" pressure which is considerably below ambient. Similarly, when the flow is attached the upwash above the body acts as an ejector and produces a larger negative pressure. For a body in an infinite stream attached flow would result in higher (more positive) base pressures, and thus less drag. The pressure distributions of Fig. 3 also show the reason for the sensitivity of the forces to the body geometry. The integrated pressures (forces) involve two areas on the bottom surface, one positive and one negative. The resulting force is therefore the small difference between two large numbers, and is very sensitive to shifts in the curve.

Another area studied was the effect of the strake depth on interference forces. Figure 4 shows that we found a continuing increase in upward forces as we increased depth. The curve for $r = 0$, no strakes is a reference line. This was the curve of greatest interference force in Fig. 2. Note also that a body with a corner radius and fitted with strakes which come even with the fuselage bottom section produces a higher interference force than the flat-bottomed body.

Extending this investigation to other classes of bodies, we used what we have here designated the "medium width body," sketched in Fig. 5. Nozzle spacings between 2.4 and 4.0 result in nozzles contained within the planform of the fuselage. This class of design is more characteristic of supersonic aircraft.

Interference forces on these bodies without strakes (Fig. 5) have much larger negative values than those for the preceding cases (Fig. 2). This is basically because of the larger area for the lower-surface pressures to affect. We found no significant effect of the corner radius or the upper-surface corner geometry for this body. The addition of strakes again produced a large positive increment in forces, and a region of unsteady flow developed for $S/D = 3.0$ and height above ground between S/D of 1.5 and 2.5. As mentioned above, this unsteady region is due to a basic upwash instability.

A survey of the effects of strake height and strake spacing were conducted at a nozzle spacing (S/D) of 4.0. Variation of the strake spacing produced some changes in the force curves, with an optimum at some intermediate spacing. In all cases significant positive forces resulted. The positive force increment due to the strakes increased with the increasing strake height up to about $\sigma/D = 0.25$. Doubling of that value produced very little change.

We also examined briefly the flow with a very large plate at the nozzle exit plane. We used a square plate $12D \times 12D$, again with a nozzle spacing of $S/D = 4.0$. Large negative forces were found without strakes, but for this "vehicle" the large positive force increments with strakes did not occur.

To analyze the observed force behavior further and to improve our modeling of IGE flows, we conducted experiments involving detailed flow surveys of the upwash without the bodies present.

Basic Upwash Characteristics

In this section we present detailed measurements of the flow properties in the ground interaction flowfield formed by dual-jet impingement and the modeling techniques that were developed to describe some regions of this flowfield. Modeling of the various components of the ground impingement flowfield relies on experimental data. Properties of the incident jet plumes have been modeled by other investigators, and a recent review of such work appears in Harsha.[17] Modeling of the jet impingement and wall jet

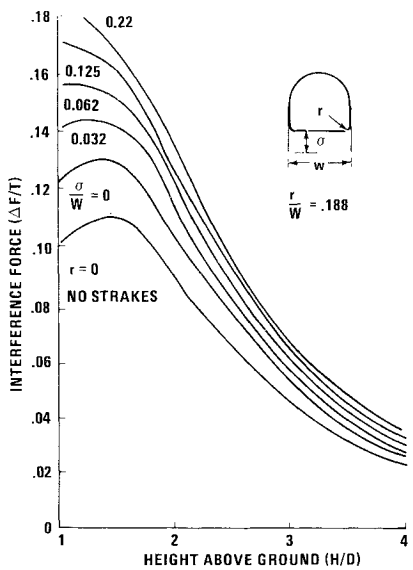

Fig. 4 Effect of strake depth on IGE forces—two-dimensional bodies.

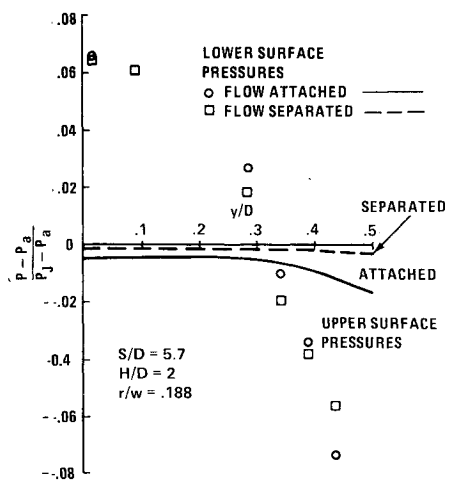

Fig. 3 Effect of flow separation on body pressure distribution.

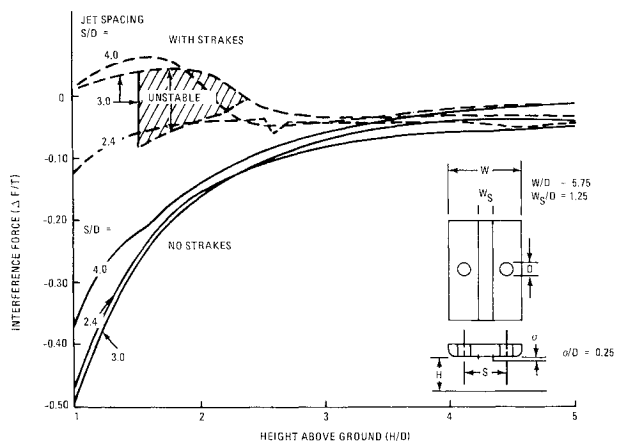

Fig. 5 Effect of jet spacing on IGE interference forces—medium width body.

formation can be based upon the work of Donaldson and Snedeker.[18] The location where wall jets from adjacent nozzles meet and form the upwash (known as the stagnation line) is the next step in the flowfield calculations. This region is described below using ground pressure profiles.

Figure 6 shows the ground pressure profile along a line passing through the two jet impact points and the centerline of the upwash. The maximum pressure in the jet impingement region (P_j) was always greater than the maximum pressure on the center of the stagnation line (P_{CS}). The dimension $y_{0.5}$ represents the half width of the pressure profile at half the maximum stagnation line pressure. Along the stagnation line the maximum ground pressure (P_m) decreases with distance (x) from the centerline.

Figure 7 shows the variation of centerline pressure on the stagnation line with nozzle spacing for a nozzle height of three diameters above ground. The curve shown for comparison was predicted by assuming that the ground pressure on the center of the stagnation line is equal to the maximum pressure that would exist in a wall jet profile at the same radial location from one of the jets if the opposite jet were turned off. The predicted curve is given by the relation

$$(P_{CS}-P_a)/(P_j-P_a)=13.78(S/D)^{-2.4} \quad (1)$$

where P_j is the stagnation pressure at the nozzle exit and P_a is ambient pressure. The constants in this equation were derived from pitot probe measurements taken in the wall jet formed by impingement of a single 10.2 cm. diameter jet. Figure 7 shows that this analysis provides an adequate prediction of the centerline ground pressure for jet spacings of about four diameters or greater. At closer nozzle spacings the measured values fall below the predicted curve. This deviation should be expected because at $S/D=4$ the stagnation line is two diameters from each jet impingement point, and this radial distance from a single impinging jet represents the beginning of the fully formed wall jet region. Hence the measured and predicted values begin to diverge, because at close jet spacings the ground flow approaching the stagnation line is not a fully formed wall jet.

The variation of maximum ground plane pressure along the stagnation line is shown in Fig. 8 for different nozzle spacings. For each spacing the maximum pressure at a given value of x, (P_m-P_a), was normalized by the centerline level. When plotted vs x/s the data for each nozzle spacing fall close to the predicted profile

$$(P_m-P_a)/(P_{CS}-P_a)=[1+(2x/s)^2]^{-2.2} \quad (2)$$

Equation (2) was derived by assuming that on the stagnation line only the component of wall jet velocity normal to the stagnation line contributes to the stagnation line pressure. The constants in Eq. (2) were obtained from wall jet measurements with a single impinging jet.

Ground pressure profiles taken across the stagnation line showed that its shape closely matched a Gaussian profile. Figure 9a shows the variation of maximum stagnation line pressure and half pressure width with nozzle height for $S/D=4$. The maximum ground pressure decreases and the width increases as the ground height increases. This general trend appeared for all jet spacings.

Integration of the ground pressure profile across the stagnation line provides a measure of the force exerted on the ground by the upwash, which can be related to the momentum flux of the upwash at ground level. If flow momentum is conserved in the upwash formation region, the momentum flux per radian of the upwash flow normal to the ground at the stagnation line can be found by integrating the stagnation line pressure profile. Using a Gaussian equation to represent this profile, integration yields

$$\dot{M}_\theta = S/2\sqrt{\pi/0.6932}(P_{CS}-P_a)y_{0.5}\left[1-\frac{y_{0.5}}{S/2}\left(1/\sqrt{0.6932\pi}\right)\right] \quad (3)$$

As shown in Fig. 9b the centerline momentum flux per radian computed from Eq. (3) using the data in Fig. 9a is almost independent of nozzle height above ground and corresponds to twice the thrust per radian of one of the incident jets. We conclude that flow momentum is conserved in the upwash formation region, and that the upwash momentum at ground level can be computed from the nozzle exit conditions.

Flow properties in the upwash were found by traversing the Kiel and static probes in the y direction at various heights (z) above ground. Figure 10 shows data obtained from a typical probe traverse across the upwash centerline. Note that the static pressure was below ambient throughout the upwash and beyond its edges. At the edges of the upwash, the Kiel pressure

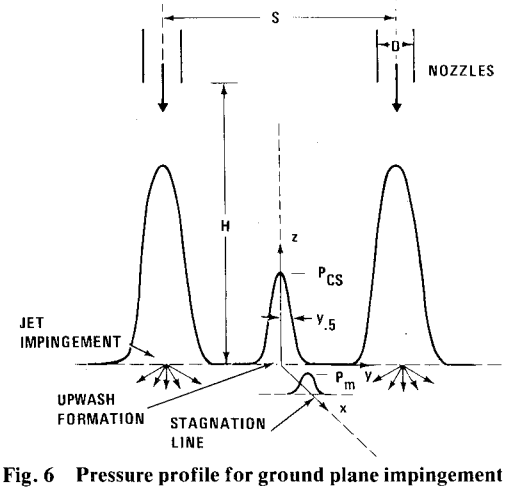

Fig. 6 Pressure profile for ground plane impingement.

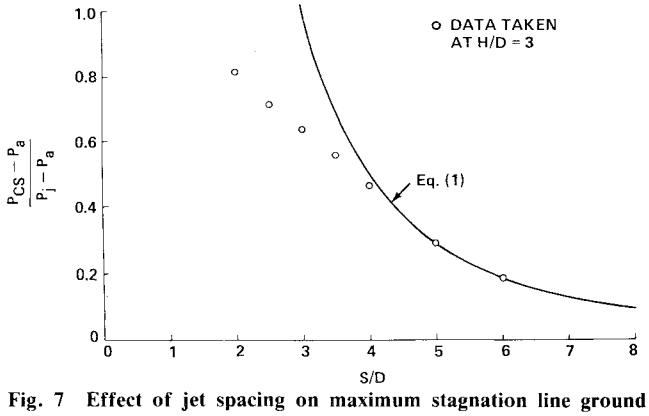

Fig. 7 Effect of jet spacing on maximum stagnation line ground pressure.

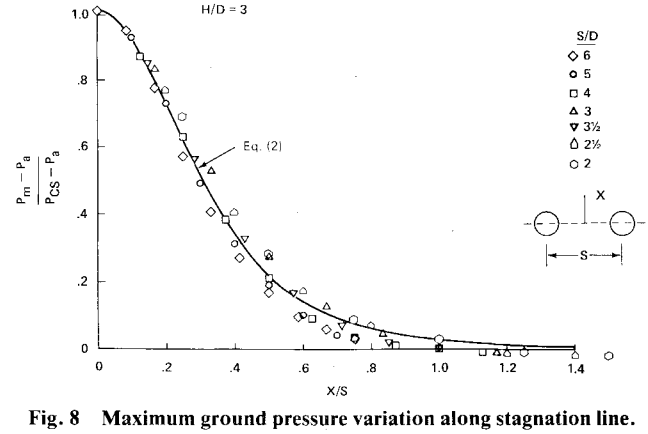

Fig. 8 Maximum ground pressure variation along stagnation line.

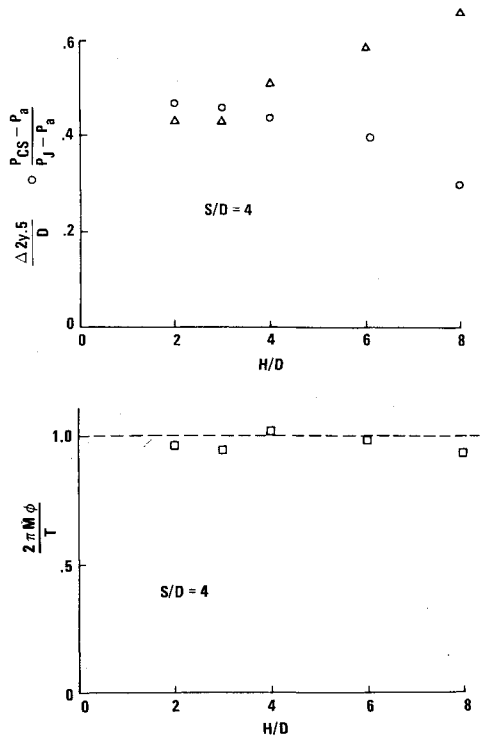

Fig. 9 Effect of nozzle height on ground properties. a) Variation of stagnation line characteristics; b) variation of integrated ground pressure force.

and static pressure readings were equal. We found that the static pressure was below ambient throughout the region between the nozzle exit plane and the ground except for a small zone just above the stagnation line. This large region of low static pressure appears to be a characteristic of multiple-jet ground impingement flows, and was found at all values of H and S that were run.

Dynamic pressure profiles across the upwash showed close agreement with a Gaussian curve. Profiles of this shape were found for nozzle separation distances down to $S/D=3$ providing the nozzle height above ground was not large enough to provide a significant interaction between the incident jets and the upwash. When the dynamic pressure profile shape is independent of height above ground, at any value of z the upwash properties on the centerline can be specified by the values of q_c/q_j and $y_{.0.25}$.

Figure 11 shows the dynamic pressure decay along the upwash centerline for $H/D=4$ at different nozzle spacings. For each spacing the values of q_c were normalized by the corresponding maximum ground pressure at the center of the stagnation line. The data are plotted vs $(S/2+z)/(S/2)$ to account for changes in the radial flow pattern in the upwash at different values of S. The data for $S/D=5$ and 6 fall along a straight line, indicating that the dynamic pressure variation along the upwash centerline can be represented by a power law decay. As the spacing is decreased the data deviate from a straight line because of interference between the upwash and the incident jet flow at this nozzle height above ground.

The variation of upwash properties on the centerline at the nozzle exit plane with jet spacing and jet height above ground is illustrated in Fig. 12. Decreasing nozzle spacing increases the exit plane maximum dynamic pressure, with not much change in upwash width, until a maximum value is reached between three and four diameters. Further decrease in nozzle spacing brings about a decrease in exit plane dynamic pressure. This variation in upwash strength with nozzle spacing reflects the same trend as the model force curves shown in Figs. 1a and 1c.

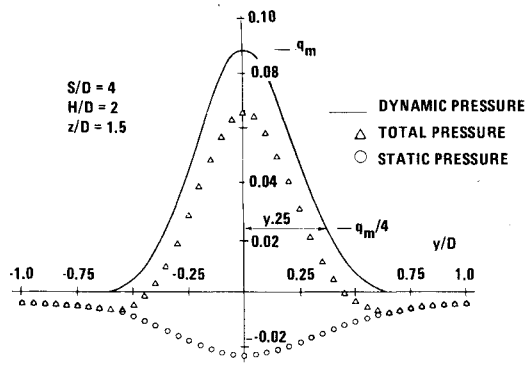

Fig. 10 Pressure profiles across upwash centerline.

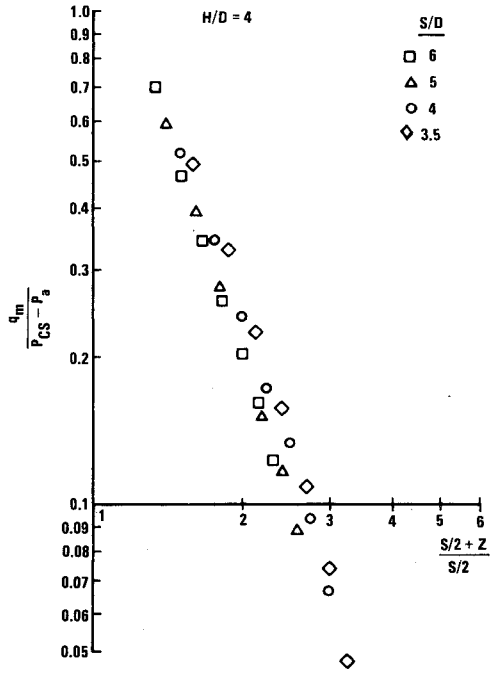

Fig. 11 Dynamic pressure decay along upwash centerline.

At low ground heights we encountered instabilities in the upwash at a nozzle spacing of three diameters. Such instabilities appeared as abnormally large fluctuations in probe readings. Kiel probe fluctuations in the upwash were generally found to be in the range of 10% of the mean value when flow conditions were stable. Unstable flow conditions increased the fluctuation level to over 50%. Unstable conditions were encountered for $S/D=3$ when H/D was decreased to less than 2½. Corresponding instabilities in ground plan pressure were noted under the same impingement conditions, indicating that the entire upwash flow was affected. These upwash instabilities occurred at the same nozzle spacing and height above ground as the observed regions of unsteady forces (Figs. 1b and 5). The cause of these instabilities is still under active investigation. Further decreases in jet spacing provided more stable upwash conditions at low ground heights, but the pressure profiles at the exit plane were somewhat unsymmetric.

The flow properties on the upwash centerline at the nozzle exit plane are also illustrated in Fig. 13, which shows curves of constant dynamic pressure on a plot of H/D vs S/D. The boundaries on the left side of this curve, labeled 7 and 10 deg, represent the conditions where the incident jets overlap shear layers before impinging on the ground. The difference in these two boundaries is the spreading angle assumed for the free jet plumes. The lower boundary corresponds to a stability limit

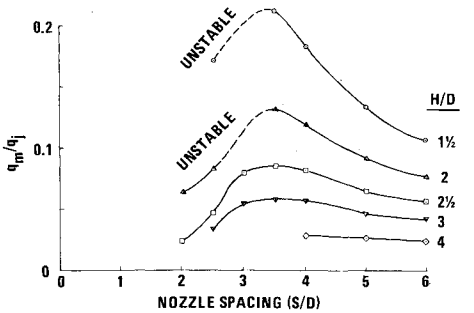

Fig. 12 Upwash properties at nozzle exit plane.

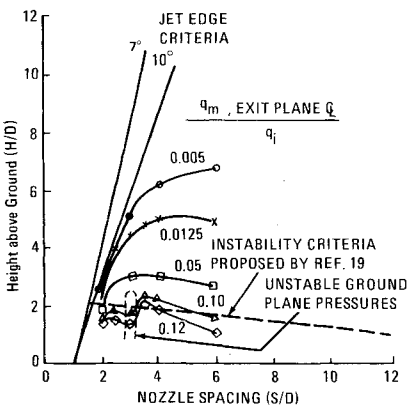

Fig. 13 Effect of nozzle spacing and height on maximum upwash dynamic pressure at exit plane.

illustrated on a similar plot presented by Hall and Rogers.[19] We found that stable impingement flows existed at lower values of H/D than they indicated; however, an unstable region does appear to exist around $S/D=3$ as illustrated by the dashed region sketched in Fig. 13.

At the closest nozzle spacing, $S/D=2$, we found that the upwash was mildly unstable at $H/D=2\frac{1}{2}$ and 3, but not for lower or higher values of H/D. Such instabilities would disappear if the symmetry of the impingement was disturbed. Misalignment of the ground plane by a few degrees would smooth out the instability described above. In addition, excessive blockage by a probe support could stabilize this type of fluctuation.

Conclusions

Forces resulting from IGE operation of a hovering V/STOL aircraft can be very sensitive to nozzle spacing and vehicle geometry. Favorable interference forces were found on bodies employing strakes to enhance "lift" near the ground. These forces increased as the nozzle spacing was decreased, attaining a maximum level between an S/D of 3 and 4. Flow instabilities were encountered with and without a model in the upwash using a nozzle spacing near three diameters at low ground heights. Nozzle spacings below 2.8 were free of this instability but produced less favorable interference forces.

Acknowledgments

A portion of this work was supported by NASA Ames Research Center under Contract NAS 2-10097. The technical monitor is D. Koenig.

References

[1] Siewert, R.F., Schmidt, L.V., Schleicher, R.A., Mazza, C.L., Brennan, T.J., and Porter, S., (VTAC) "U.S. Navy V/STOL Technology Assessment, Vol. I Executive Summary," Naval Air Systems Command, June 1975.

[2] Platzer, M.F. and Margason, R.J., "Prediction Methods for Jet V/STOL Propulsion Aerodynamics," *Journal of Aircraft,* Vol. 15, Feb. 1978, pp. 69-77.

[3] *Proceedings of the Naval Air Systems Command Jet V/STOL Propulsion Aerodynamics Workshop,* Arlington, Va., July 28-31, 1975, M.F. Platzer, ed.

[4] *Proceedings of the AIAA/NASA Ames V/STOL Conference,* Palo Alto, Calif., June 6-8, 1977.

[5] *Proceedings of the Project Squid Workshop on Engine-Airframe Integration,* U.S. Naval Academy, Annapolis, Md., May 1977, M.F. Platzer, ed.

[6] *Proceedings of the V/STOL Aerodynamics Workshop at the Naval Postgraduate School,* Monterey, Calif., May 16-18, 1979.

[7] Hill, W.G., Jr., and Jenkins, R.C., "Ground Impingement of a Fan Jet Exhaust Plume," Grumman Research Dept. Memorandum RM-653, May 1978.

[8] Wooten, W.H. and Hoff, G.E., "Deflected Exhaust Jet Effects on V/STOL Fighter Performance," General Electric Rept. R73AEG279, July 1973.

[9] Gentry, C.L. and Margason, R.J., "Jet Induced Lift Losses on VTOL Configurations Hovering In- and Out-of- Ground Effect," NASA TN D 3166, 1966.

[10] Spreeman, K.P. and Sherman, I.R., "Effects of Ground Proximity of a Simple Downward-Directed Jet Beneath a Flat Surface," NASA TN 4407, 1958.

[11] Kuhn, R.E., "An Empirical Method for Estimating Jet Induced Lift Losses of V/STOL Aircraft Hovering in and out of Ground Effect," Aerospace Mass Properties Analysis Inc., Norristown, Pa., Rept. R-AMPAC-105, Dec. 1978.

[12] Siclari, M.J., Hill, W.G., Jr., and Jenkins, R.C., "Investigation of Stagnation Line and Upwash Formation," AIAA Paper 77-615, AIAA/NASA Ames V/STOL Conference, Palo Alto, Calif., June 1977.

[13] Siclari, M.J., Aidala, P., Hill, W.G., Jr., Jenkins, R.C., Migdal, D., and Wohllebe, F., "Development of a Methodology to Predict the Ground Footprint of V/STOL Aircraft," Grumman Aerospace Corp., Rept. PDR 698-4, Oct. 18, 1977.

[14] Hill, W.G., Jr., "Propulsion Induced Effects for VTOL Aircraft in Ground Effect," Project Squid Workshop on Engine-Airframe Integration, U.S. Naval Academy, Annapolis, Md., May 1977 (also available as Grumman Research Dept. Memorandum RM-634J, June 1977).

[15] Hill, W.G., Jr., and Jenkins, R.C., "A Study Upwash Impingement on the Vehicle for a Two Jet Type A Design," Paper presented at the Workshop on V/STOL Aerodynamics, Naval Postgraduate School, Monterey, Calif., May 16-18, 1979.

[16] Wohllebe, F.A. and Migdal, D. "Some Basic Test Results of V/STOL Jet Induced Lift Effects in Hover," AIAA Paper 79-0339, AIAA 17th Aerospace Sciences Meeting, New Orleans, La., Jan. 15-17, 1979.

[17] Harsha, P.T., "Free Turbulent Mixing: A Critical Evaluation of Theory and Experiment," AEDC TR-71-36, Feb. 1971.

[18] Donaldson, C. DuP. and Snedeker, R.S., "A Study of Free Jet Impingement, Part I, Mean Properties of Free and Impinging Jets," *Journal of Fluid Mechanics,* Vol. 45, Part 2, 1971, pp. 281-319.

[19] Hall, G.R. and Rogers, K.H., "Recirculation Effects Produced by a Pair of Heated Jets Impinging on a Ground Plane," NASA CR 1307, May 1978.